ORGANOPHOSPHORUS RADICALS IN NATURAL APATITES $Ca_2(PO_4)_3(F,OH)$

L. G. Gilinskaya, Yu. N. Zanin, R. G. Knubovets, T. A. Korneva, and V. P. Fadeeva

UDC 549.753.1:548.3:635.537:535.34

ESR spectroscopy was used to identify new radicals in natural sedimentary carbonate-containing F,OH-apatites with ^{31}P splitting for phosphinyl (PL_2), phosphoryl (PL_3), and phosphoranyl radicals (PL_4). The ESR spectral parameters were determined and compared with those for the PO_3^{2-} sites previously studied in apatite. The correlation of the new sites with the presence of hydrocarbon groups in the samples studied, established by chemical and thermal analysis and IR spectroscopy, indicated that the new radicals are organophosphorus complexes.

The ESR study of the crystal chemical features of natural apatites led to the identification of a paramagnetic site of the PO_3^{2-} electronic type ($S = ½$, $J = ½$) with characteristic ^{31}P line splitting [1, 2]. The reason for the formation of this site in the given matrix is the isomorphic introduction of U^{4+} and Th^{4+} actinide ions into $Ca^{2+}II$ positions, which displace atomic ligands in the first coordination sphere, specifically, one of the oxygen atoms OIII(2), OI(1), and OII(1) of the PO_4^{3-} tetrahedra. This results in the formation of a PO_3^- fragment. The subsequent capture of an electron by this fragment leads to the formation of a PO_3^{2-} paramagnetic site [3-5]. Depending on which of the oxygens of the PO_4^{3-}tetrahedron is displaced (OIII or OI(II)), two types of sites ($PO_3^{2-}(1)$ and $PO_3^{2-}(2)$) are formed with intensity ratio $I_1:I_2 = 2:1$, which corresponds to the crystal structural parameter of apatite. Furthermore, the nature of the actinide ion replacing $Ca^{2+}II$ (U or Th) affects the various ESR spectral parameters for PO_3^{2-} and other characteristic features. Thus, the lines in the spectrum of $PO_3^{2-}(Th)$ have characteristic superhyperfine structure due to the hydrogen nuclei of the OH^- group on the 6_3 axis of apatite. This indicates that Th is found as $(ThOH)^{3+}$ complexes, while uranium is found as UO_2 or UO^{2+} complexes. Thus, four types of PO_3^{2-} site types were found in the structure of apatite: $PO_3^{2-}(U)_1$, $PO_3^{2-}(U)_2$, $PO_3^{2-}(Th)_1$, and $PO_3^{2-}(Th)_2$ [5]. The study of apatites of different origin led to the conclusion that the PO_3^{2-} sites are detected in all the genetic varieties containing U and Th ions and their intensity is proportional to the content of these ions.

However, further study showed that these PO_3^{2-} paramagnetic sites do not exhaust the types of radicals displaying ^{31}P splitting detected by ESR spectroscopy in natural apatites. In a certain genetic group, namely, in sedimentary phosphorite apatites (and only in this group), a number of other types of paramagnetic sites with ^{31}P splitting were detected. This is the subject of the present communication.

Natural polycrystalline samples of sedimentary apatites of various phosphorite deposits in the Khubsugul' basin in the USSR and Mongolia, Kartau basin in Kazakhstan, Georgina basin in Australia, Aravalli basin in India, phosphorium formation in the United States, and Irsym (Prisayan'e) were studied by ESR spectroscopy at 290 K using RÉ-1306, Varian E109E, and SE-X Radiopan spectrometers, $\lambda = 3$ cm, $f_{mod} = 100$ kHz. Prior to taking the ESR spectra, the samples were irradiated using cobalt-60 γ-radiation (2-4 Mrad dose). Furthermore, IR spectra were taken on an Bruker Fourier-transform IFS-112 and Karl Zeiss Specord--75IR spectrometers. Subtraction of KBr (when the samples were prepared as KBr pellets) and deduction of the base line were carried out on the IFS spectrometer. An additional recorder with expansion of the ordinate was used on the Specord-75IR spectrometer. Thermal and chemical analyses were carried out and ENDOR and ^{31}P MAS-NMR spectra were taken. The thermal

OIGGiM and Institute of General Chemistry, Siberian Branch, Russian Academy of Sciences, Novosibirsk and GIGKhS, MG of the USSR, Moscow. Translated from Zhurnal Strukturnoi Khimii, Vol. 33, No. 6, pp. 109-122, November–December, 1992. Original article submitted December 1, 1991.

0022-4766/92/3306-0859$12.50

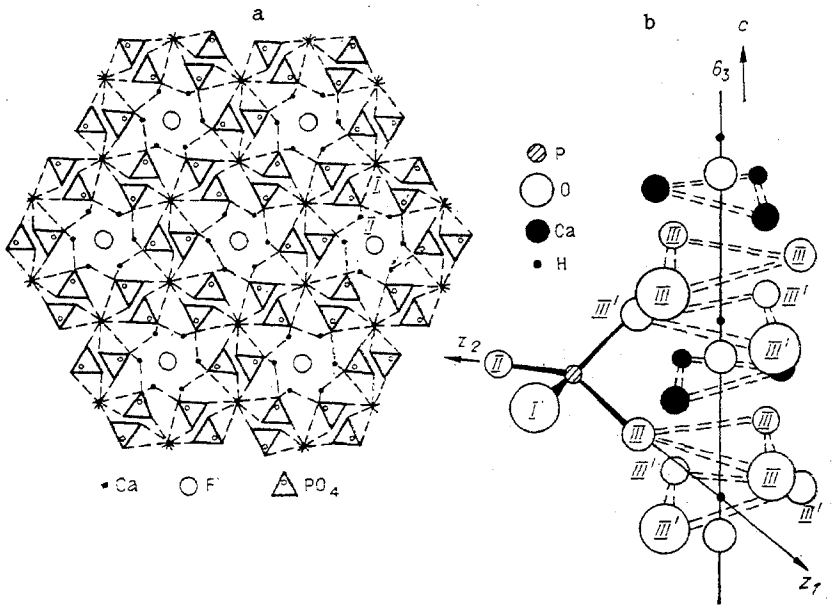

Fig. 1. Crystal structure of apatite: a) projection onto the (0001) plane, b) arrangement of ions about the six-fold screw 6_3 axis (from the work of Young [8]).

analysis was carried out on an OD-103 derivatograph manufactured in Hungary under the following experimental conditions: linear heating at a rate of 10 deg/min in the air with an alumina standard for a sample 100 mg. The TG sample was 50 mg. DTA) 1/5 and DTG) 1/5. In addition to the ordinary chemical analysis, we determined the content of organic elements C, H, and N in several samples by oxidative decomposition at 1100°C in an automatic Hewlett-Packard analyzer (mod. 185) in the presence of an efficient oxide catalyst [6].

The chemical compositions of the apatites studied are given in Table 1, which shows that the samples are carbonate-containing F,OH-apatites. The presence of organic matter is noted.

Crystalline Structure. Apatite, $Ca_5(PO_4)_3(F,Cl,OH)$, crystallizes with hexagonal symmetry in the $P6_3/m$ space group. Monoclinic varieties with the $P2_1/b$ space group (Cl-apatite and OH-apatite) are rarely encountered in nature [7]. Characteristic features of the crystal structure are: 1) presence of two Ca^{2+} positions with different coordination, namely, $Ca^{2+}I$ (C_3 symmetry, CaO_9) and $Ca^{2+}II$ (C_{1h} symmetry, CaO_6F), which are connected to each other by means of orthophosphate PO_4^{3-} groups (Fig. 1a); 2) presence of different halide ions, namely, F, OH, Cl, and oxygen in different valence forms (O^{2-} and O^-) as well as vacancies on the channel axis (the 6_3 axis) formed by OIII and OIII′ atoms of PO_4 tetrahedra (Fig. 1b). The complexity of the apatite structure, in particular, the saturation of the 6_3 axis by impurities and vacancies leads to the formation of various defects both on this axis [2, 9] and in the different structural connecting elements, in particular, the $PO_3^{2-}(Th)_1$ site mentioned above [5]. We also encounter displacement of atoms, the breakdown of structural elements, and the formation of complexes such as VO^{2+} [11]. More than 30 different sites have now been identified in the apatite structure only by ESR spectroscopy, which indicates the considerable crystal chemical possibilities for the apatite structure relative to the formation and stabilization of defects.

ESR Spectra. This group of apatites exists in nature only in polycrystalline form. Therefore, let us briefly examine the ESR spectra of polycrystalline PO_3^{2-}(U, Th) since they overlap the new spectra studied in this work. A detailed study of the ESR spectra of the PO_3^{2-} sites due to the presence of uranium or thorium in apatite monocrystals showed that there are 24 magnetic complexes in the structure (six of each type with pairwise equivalence 3 × 2). Even along the major axes, the spectrum recorded is rather complex [2, 5]. The situation is simplified somewhat if only one isomorphic actinide ion U or Th is present or absolutely predominates, which is rather rare. As a rule, this geochemical pair is always present together and uranium usually predominates. The ESR spectra of the PO_3^{2-} sites in polycrystalline apatites are somewhat simplified since only two orientations are seen: θ = 0 and 90°. The ratio of the intensities of the two types, $PO_3^{2-}(1):PO_3^{2-}(2)$ = 2:1 still holds. Only the $PO_3^{2-}(1)$ type is seen rather frequently due to the broadening effects in

TABLE 1. Chemical Composition of the Phosphorite Apatites Studied

Sample No.	P_2O_5	TiO_2	SiO_2	Al_2O_3	Fe_2O_3*	K_2O	Na_2O	CaO	MgO	MnO	H_2O^-	H_2O^+	CO_2	F	Σ for $O=F_2$	Calcination loss
1	39,50	—	2,72	—	0,20	0,10	0,28	55,01	0,05	—	0,01	—	0,21	3,33	100,01	1,13
2	36,67	0,03	6,17	0,10	—	0,06	0,43	52,01	1,43	0,03	n.d.	n.d.	0,69	3,07	99,50	3,00
3	40,75	—	1,10	—	0,05	0,12	0,52	54,58	0,10	—	0,06	—	0,42	3,38	99,66	0,44
4	36,57	0,03	3,13	0,43	0,02	0,16	0,74	55,42	0,44	0,03	n.d.	n.d.	1,60	3,65	100,69	2,56
5	35,70	0,03	2,34	0,19	—	0,05	0,81	55,32	0,38	0,03	n.d.	n.d.	2,85	3,96	100,00	4,76
6	34,95	0,03	5,03	0,20	—	0,08	0,81	52,98	0,34	0,03	n.d.	n.d.	3,19	3,65	99,76	4,84
7	38,40	0,05	2,50	0,03	0,15	0,18	0,56	52,76	0,16	0,01	0,14	1,20	1,45	3,96	99,89	n.d.
8	36,50	0,06	3,40	0,22	1,00	0,25	0,63	51,67	0,27	0,01	0,30	1,26	1,10	3,85	98,91	n.d.
9	39,40	0,05	1,50	0,26	0,20	0,18	0,37	54,39	0,10	0,02	0,20	0,50	1,65	3,90	101,08	n.d.
10	38,30	0,03	3,60	—	0,26	0,14	0,29	54,50	0,05	0,06	0,20	0,32	1,10	2,91	100,54	n.d
11	40.27	—	0.70	0.15	—	0.06	0,33	55,56	—	n.d.	0,50	—	0.17	3.45	99.80	n.d.

*Total iron. The minus sign indicates absence, n.d.) not determined. Samples from the Khubsugul' basin (1-3), from the Phosphorium formation (4-6), Georgina formation (7-9), Arava lli formation (10), and Ir sym display (11).

TABLE 2. ESR Spectral Parameters[a] of Phosphorus-Containing Radicals in Apatite

Center	^{31}P hyperfine splitting, mT			$g_\parallel$	$g_\perp$	g_{iso}	[b] c_s^2	c_p^2	$\lambda=c_p^2/c_s^2$	Reference
	$A_\parallel$	$A_\perp$	A_{iso}							
A	30,3	—1,1	9,4	2,00	2,012	2,008	0,025	1,036	40,6	Present work
B	74,4	60,2	64,9	1,993	2,004	2,000	0,176	0,470	2,76	»
C	98,6	82,5	87,9	1,972	1,989	1,983	0,239	0,531	2,22	»
$PO_3^{2-}(U)_I$	60,5	46,4	51,5	1,988	2,005	2,002	0,139	0,465	3,34	[1]
$PO_3^{2-}(U)_I^*$	62,9	48,8	53,5	2,008	2,005	2,006	0,145	0,465	3,20	Present work
$PO_3^{2-}(U)_2$	74,5	60,0	64,8	1,991	2,004	1,999	0,176	0,479	2,72	[1, 5]
$PO_3^{2-}(Th)_I$[c]	75,6	59,4	64,6	1,992	2,006	2,001	0,176	0,544	3,09	[5]
$PO_3^{2-}(Th)_2$	97,0	81,0	89,0	1,999	2,000	1,999	0,230	0,500	2,16	[5]

[a]Parameters calculated using the Breit–Rabi formula; the error in the determination of A was ±0.05 mT and the error in the determination of g was ±0.002. The minus sign for $A_\parallel$ in the spectrum of A was taken according to Kerr et al. [15]. [b]The spin density in the 3s and 3p phosphorus orbitals were determined using A_0 = 367.6 mT, 2B = 20.2 mT from our previous work [30]. [c]Hyperfine splitting with the ^1H nucleus recorded with the following parameters: $A_\parallel$ = 1.0 mT, $A_\perp$ = 0.7 mT.

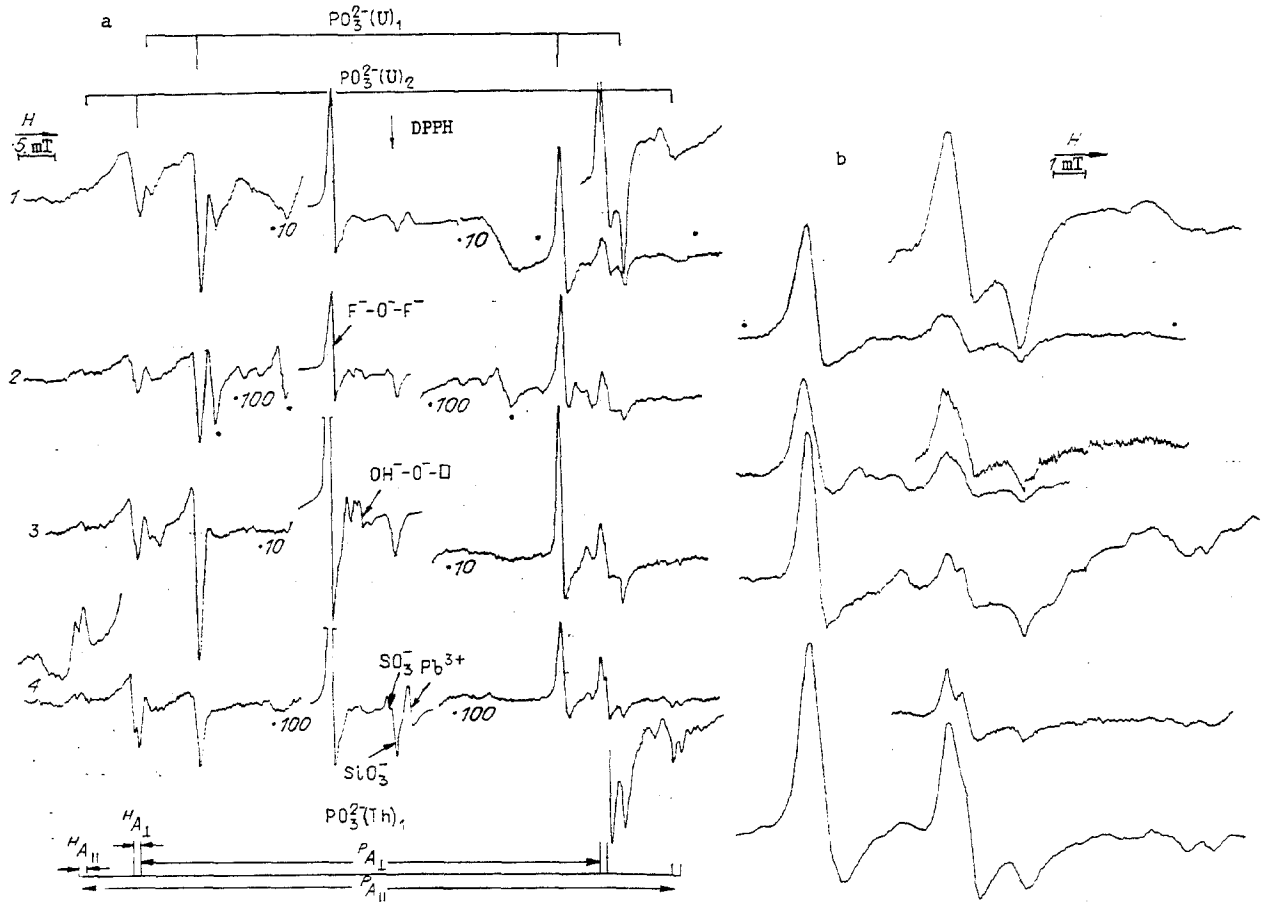

Fig. 2. ESR spectra of magmatogenic polycrystalline apatites with equal intensity ratio for the $PO_3^{2-}(U)_1$ and $PO_3^{2-}(Th)_1$ sites: a) samples from the deposits at Khibina (1), Slyudyank (2), Kanku (3), and Niryandzh (4). b) upfield spectral components. K) calcite.

structures deformed by defects. Figure 2 shows the ESR spectra of polycrystalline magmatogenic apatites with different ratios of the intensities of the $PO_3^{2-}(U)_1$ and $PO_3^{2-}(Th)_1$ sites with an increase in the fraction of the latter site to almost equal the fraction of the former in going from sample 1 to 4. The spectrum of $PO_3^{2-}(Th)_1$ spectrum is deformed by lines of the $PO_3^{2-}(U)_2$ spectrum due to overlap, especially in the case of a high intensity of $PO_3^{2-}(U)$ sites. Evaluation of the intensity ratio for these two sites carried out for the monocrystal is 5:3 for sample 1, 5:1.5 for sample 2, 19:3 for sample 3, and 1:1.5 for sample 4.

The PO_3^{2-} sites in this group of sedimentary apatites are characteristic for cathagenically transformed types.* Figure 3 gives the ESR spectra of three of these sedimentary apatites, which are a superposition of the abovementioned $PO_3^{2-}(U)_{1,2}$ and $PO_3^{2-}(Th)_{1,2}$ sites with some new sites designated A, B, and C. The spectrum of sample 11 (numbering in accord with Table 1) with a high content of U and Th clearly shows these features. An intensity for $PO_3^{2-}(U)_1$ in sample 1 much less than for the $PO_3^{2-}(Th)_1$ site is characteristic (^1H hyperfine splitting). In this case, both spectra are superposed onto the $Mn^{2+} \rightarrow Ca^{2+}I$ spectrum. The lines of the new spectra, especially of b, which overlaps and distorts the spectrum of $PO_3^{2-}(Th)_1$ have significant intensity in sample 6 with relatively low intensity of the PO_3^{2-}-$(U)_1$ site and very low intensity of the $PO_3^{2-}(Th)_1$ site. The intensity of spectra A, B, and C do not correlate with the content of the actinide ions in the matrix (Table 3). They are

*Cathagenesis is a physicochemical process for the transformation of sedimentary soils in the Earth's crust at low temperatures (up to 300°C) and pressures (up to 2500-3000 kg/cm^2).

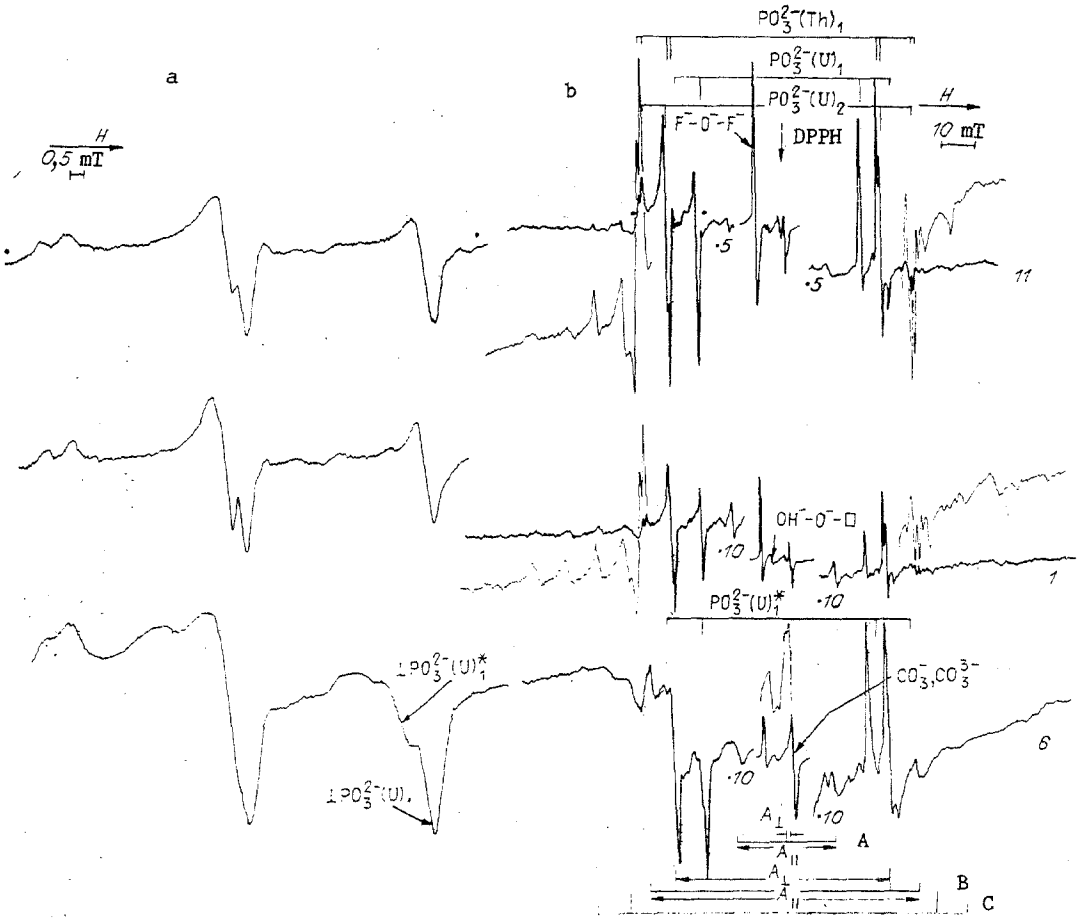

Fig. 3. ESR spectrum of polycrystalline sedimentary apatites: a) downfield components of the spectra, b) samples Nos. 11, 1, and 6 in accord with the numbering in Table 1. The spectrum for $Mn^{2+} \rightarrow Ca^{2+}I$ overlaps the spectrum of sample 1.

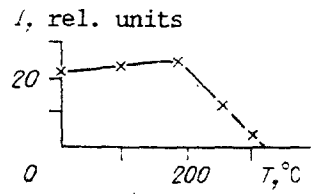

Fig. 4. Temperature dependence of the intensity (relative units) of the ESR spectrum of the phosphoryl radical $\dot{P}L_3$ in sample No. 5 (the roasting time at these points is 1.5 h).

detected together and, as a rule, spectrum B has the highest intensity. $PO_3^{2-}(Th)_1$ sites of various intensity virtually always accompany spectrum B. The lines of the new spectra appear after γ-irradiation or increase in the case when γ-ray sources such as U or Th are present in the structure and, finally, recombine over time.

The parameters of spectra A, B, and C are given in Table 2 along with the data for $PO_3^{2-}(U)_{1,2}$ and $PO_3^{2-}(Th)_{1,2}$ radicals in apatite. We should note the high anisotropy of the hyperfine splitting in spectrum A and, as a consequence, the large difference in the ratio

TABLE 3. Intensity of Paramagnetic PL_3 Radicals and Some Analytical Parameters of the Apatites Studied

Sample No.	ESR intensity of PL_3 radical, rel. units	Mass loss, Δm, %			Presence of C–H stretching vibrations in IR spectrum	Chemical analysis			Sample color	U, %	Th, %
		320°	400–550°	ΣOM		ΣC, %	C_{org}, %	calcination loss			
1	190	0,3	0,5	0,8	Strong	0,75	0,69	1,13	Black	$2{,}0\cdot10^{-3}$	$1{,}4\cdot10^{-4}$
2	158	0,4	2,0	2,4	»			3,00	»	$0{,}8\cdot10^{-3}$	$8{,}0\cdot10^{-4}$
3	76	0,15	—	0,15	+	0,65	0,54	0,44	White	$1{,}7\cdot10^{-3}$	$0{,}6\cdot10^{-4}$
4	65	+	—	+	+			2,54	Gray	Not det.	Not det.
5	262	0,7	2,3	3,0	Not studied			4,66	Black	»	»
6	180	0,4	0,6	1,0	Strong	1,42	0,54	4,74	»	$1{,}2\cdot10^{-3}$	$1{,}0\cdot10^{-4}$
7	90	+	—	+	+			Not det.	Gray	$1{,}3\cdot10^{-3}$	$1{,}0\cdot10^{-4}$
8	70	+	—	+	+			»	White	Not det.	Not det.
9	—	—	—	—	Not studied			»	»	»	»
10	+	+	—	+	+			»	Gray	$4{,}0\cdot10^{-4}$	$9{,}0\cdot10^{-4}$
11	+	+	—	0,5	+			»	Pink	$1{,}5\cdot10^{-2}$	$1{,}4\cdot10^{-4}$

Note: Minus sign indicates the lack of an effect, while a plus sign indicates the presence of an effect without estimation, which was not carried out due to superposition with side effects. The determination of U was carried out by a luminescence laser method, while thorium was determined photocalorimetrically using the arsenado-3 reagent with separation of interfering impurities on KU-2 cation-exchange resin (carried out by analytical technician Z. V. Malyasova).

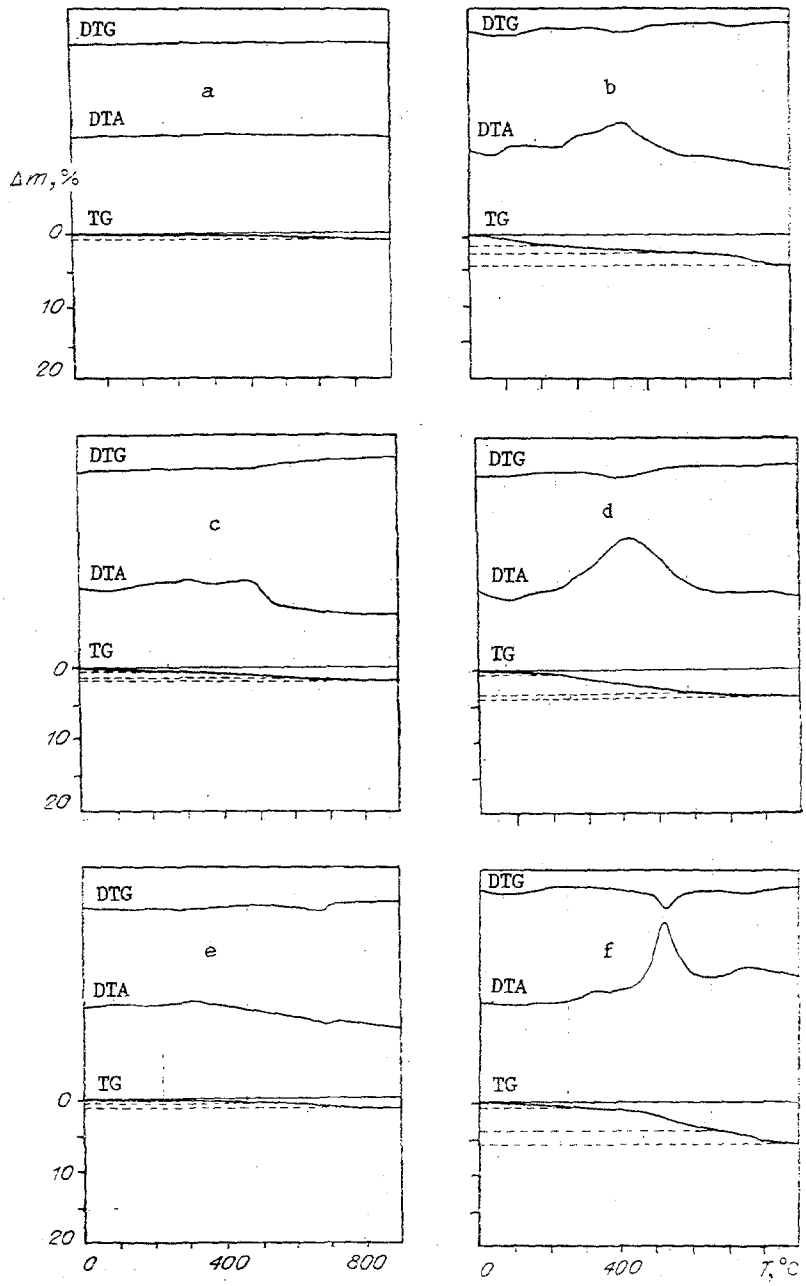

Fig. 5. TG–DTG–DTA curves of phosphorite apatites: a) sample No. 4, b) 6, c) 1, d) 2, e) 3, f) 5. The sample mass was 100 mg, TG) 50 mg, DTA) 1/5, DTG) 1/5.

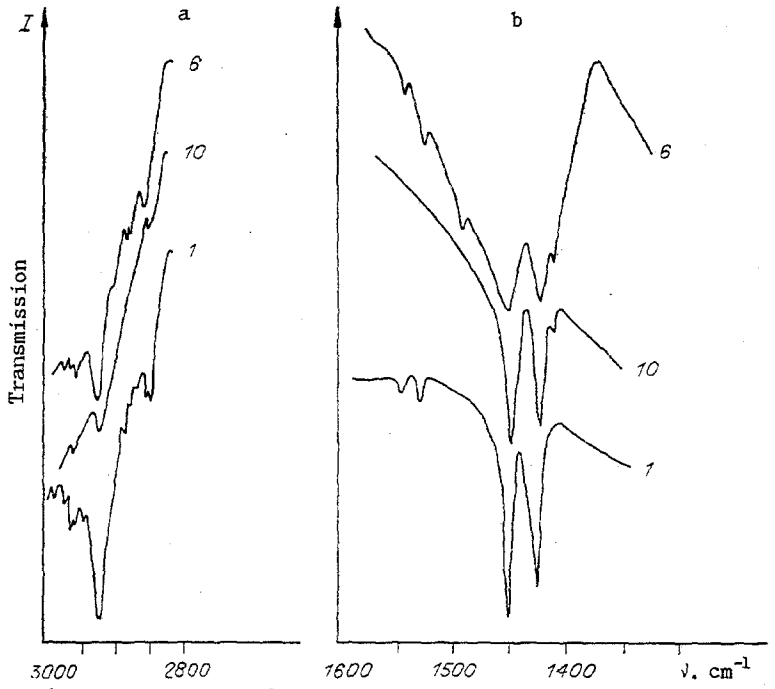

Fig. 6. IR spectra of samples Nos. 1, 10, and 6 in the region of the carbon–hydrogen bond stretching vibrations (a) and region for vibration of the carbonate ions (b).

of the spin densities in the phosphorus 3p and 3s orbitals: 3p/3s = 41. These are characteristic features of phosphinyl radicals, $\dot{P}L_2$: $\dot{P}F_2$, $\dot{P}Cl_2$, $\dot{P}(OEt)_2$, $\dot{P}(OMe)_2$, $\dot{P}H_2$, and $\dot{P}(Ph)_2$.

Spectrum B has parameters similar to those for $PO_3^{2-}(Th)_1$ sites but it lacks hyperfine lines and the linewidth is somewhat greater than for PO_3^{2-}. Analysis of the parameters obtained and the 3p/3s ratio = 2.8 indicates that the spectrum results from phosphoryl radicals, $\dot{P}L_3$: $\dot{P}O_3^{2-}$, $\dot{P}(OMe)_3$, $\dot{P}(OEt)_3$, $(MeO)_2\dot{P}O$, and $EtO\dot{P}(O)O^-$. Spectrum C could not be reliably identified due to its low intensity and overlapping. According to our calculation (see Table 2), this spectrum may be due to a phosphoranyl radical $\dot{P}L_4$ but we might also expect a dimeric radical based on the magnitude of the hyperfine coupling constant.

Figure 4 gives the results for a study of the thermal annealing of the radicals studied in the case of the phosphoryl radical, $\dot{P}L_3$ in sample 5 as the most intense. The temperature for annihilation of this radical (as for the other two) lies in the temperature range from 315 to 330°C. The PO_3^{2-} radicals in apatite, as a rule, as shown in our previous work [2], disappear at 430-450°C.

The apatite samples were studied by other methods into to obtain a more concrete notion of the shape of the observed radicals and clarify their nature.

Thermal Analysis. Differential thermal analysis (DTA) and thermogravimetry (TG) were used to record the presence, type, and amount of organic matter.

Phosphorite apatites are thermally inert up to 1100°C, i.e., they do not display effects on the DTA curves and there is virtually no mass loss upon heating (Fig. 5a, sample 9). The endothermal and exothermal effects on the DTA curves and their corresponding mass losses on the TG curves are related to the presence of impurities.

The apatites studied may be divided into two groups relative to their thermal behavior. Group 1 (Nos. 1-3, 5, 6, and 9) are characterized by the loss of the natural moisture content at 100°C (adsorbed water), exothermal effects at 300-500°C related to the removal (burn-off) of organic matter, and endothermal effects at 680-740°C due to the decomposition of the calcium carbonate mechanical impurity.

Comparison of the thermal behavior of the samples of this group revealed several differences. Thus, the DTA curve for sample 6 (Fig. 5b) shows a slight endothermal effect with maximum at 100°C (1.25%) and expanded exothermal effect with maxima at 320 and 440°C due to burn-off of organic matter (OM) and oxidation of the CH groups (1%). The gradual depression on the DTG curve corresponding to this effect indicates a slow oxidation process and removal of the volatile compounds as CO_2 and water. The "oxidative" profile of the sample [12] is most similar to the humus stage of coal of brown coals or lignite.

The DTA curve of sample 1 (Fig. 5c) shows an exothermal effect also with two maxima (320 and 490°C) but with lower intensity (0.8%). The second maximum is shifted toward higher temperatures, which indicates greater carbonification of the organic matter, more precisely, a portion of this matter. Sample 2 (see Fig. 5d) is analogous to sample 1 but the exothermal effect of the oxidation of OM is much stronger (2.4%). The DTA curve in sample 5 (Fig. 5f), similarly to the previous samples, has a weak endothermal effect at 100°C, weak exothermal effect at 320°C, and strong exothermal effect at 520°C, indicating rapid combustion, as well as a sloping extended exothermal effect at 740°C. The mass loss corresponding to the first two exo effects is 3.0%, while the mass loss corresponding to the third exo effect is 2.0%. The organic matter is close to sapropelite or humito-sapropelite [13] and has a high hydrogen content and loss of volatile components. All these samples are black, i.e., the OM is apparently macroscopic.

The DTA curve for sample 3 in this group (see Fig. 5e) has only a weak exothermal effect for oxidation at 320°C, while the TG curve has a slight gradual decline at 300-550°C. The mass loss in this sample is 0.15%. In contrast to the previous samples, this sample is white.

The thermal behavior of Group 2 (Nos. 4, 7, 8, 10, and 11) is different. Their TG curves show a gradual mass loss from 20 to 1000°C with Δm from 0.5 to 0.9%. However, only a weak exo effect for the burn-off of OM is observed at 320°C. The decrease in the mass of these samples is related to the presence of water and volatile components. Thus, the mass loss in the range of the exo effect at 320°C cannot be determined quantitatively. These samples are not black.

Thus, a weak exo peak for the burn-off of OM containing CH groups is found for all these samples except sample 9. The intensity of this peak correlates with the ESR data (see Table 3). The burn-off temperature of this portion of the OM corresponds to the temperature of the annihilation of the ESR sites studied. Furthermore, the organic matter with different extents of carbonification in a series of samples, which binds the adsorbed water (100°C), is a mechanical mixture and gives a black color. It is not excluded that, as noted below, this portion of the OM is held by the apatite surface. We note that the black color of the samples disappears after roasting above 500°C.

IR bands for the samples studied for carbon–hydrogen vibrations are found at 2926, 2960, 2855, and 2865 cm^{-1}. These bands are strongest in the spectrum of sample 1, which also has a strong ESR spectrum (see Table 3, sample 5 with the strongest ESR spectrum was not studied by IR spectroscopy). Somewhat lower intensity is found in the IR spectrum of sample 6. The weakest intensities are found in the spectrum of sample 10 (Fig. 6a). Table 3 gives the IR spectral data for the C–H stretching vibrations.

The deformation bands of the carbon–hydrogen bonds lie in the region for carbonate ions found in the apatite structure. Figure 6b shows how the lineshape for the bands in this segment of the spectrum differ. The strong broadening of the lines in the spectrum require further clarification. According to literature data, the frequencies and intensities of the bands for the stretching and deformation vibrations of carbon–hydrogen bonds in organophosphorus compounds depend significantly on the compound type [14].

RESULTS AND DISCUSSION

New radicals with ^{31}P splitting were identified by ESR spectroscopy (see spectra A, B, and C in Fig. 3). Thee radicals always accompany organic matter in the samples studied as found by chemical and thermal analysis and IR spectroscopy. Unfortunately, the sparse information provided by these methods permitted us only to obtain only the qualitative composition of the organic matter (presence of C–H bonds). On the other hand, the low concentration of organic matter (for these methods) made a clear relationship of these data difficult to obtain and only indicated the abovementioned correlation of the ESR data with the weak exo peak at 320°C and the IR spectra (see Table 3). The high sensitivity of ESR spectroscopy permitted us to detect the formation of new complexes in apatite. The observed characteristic splitting in the ESR spectra and 3p/3s ratios as well as the reported data on phosphinyl, phosphoryl, and phosphoranyl radicals with organic molecules in the coordination second sphere [15-17] indicated that spectra A, B, and C in these apatites are due to different types of organophosphorus radicals. Samples especially washed to eliminate calcium mineral traces according to the method described by Veiderma [18] and Silverman [19] and taken from samples taken from different deposits over the world but of identical

origin show the same ESR spectra (A, B, and C). Hence, these spectra are related to the apatite structure. This hypothesis is supported by the finding that the $PO_3^{2-}(U)_1$ has different parameters in samples with strong organophosphorus radical spectra (see Fig. 3, spectrum of $PO_3^{2-}(U)_1^*$), which may be due to a change in its immediate environment in the apatite structure resulting from the presence of these radicals. The dependence on the uranium content still holds. It is interesting that the black samples remain black even after washing, i.e., the carbonified organic matter detected by the thermal analysis at 400-550°C is rather stable and most likely is attached to the apatite surface.

The following radicals were examined as candidates responsible for the observed ESR spectra: $\dot{P}(OR)_2$ for spectrum A, $\dot{P}(OR)_3$, $O\dot{P}(OR)_2$, and $OPO(OR)$ for spectrum B, and $\dot{P}(OR)_4$ and $OPO(OR)_3$ for spectrum C, where R = CH_2, CH_3, or C_2H_5. Radicals such as $\dot{P}(CH)_3$, where the CH groups are directly bound to phosphorus were excluded since we should have observed further splitting of the spectral lines of about 1-4 G due to coupling with ^1H nuclei [16]. The joint observation spectra A, B, and C may be attributed to an inevitable sequence of radiation chemical reactions upon irradiation of samples containing organophosphorus species to give at least three types of radicals [15].

We attempted to determine the precise form of the observed radicals, specifically, the type of organic group (CH_2, CH_3, or C_2H_5) and number of such groups in the actual complex. The samples were studied by ENDOR spectroscopy.† However, the low intensity of the paramagnetic sites (~10^{16} spins/g), especially of $P(OR)_2$, did not permit us to detect the expected splitting from the ^1H nuclei on the equipment used. For this reason, the ^{31}P MAS--NMR spectrum showed only a single resonance peak with weak side-bands an isotropic chemical shift σ = 2.8 ppm from the PO_4^{3-} groups. Organophosphorus groups, similar to the distorted tetrahedral PO_3^{2-} sites, were not detected in the ESR spectra.

Table 3 gives the results of our calculation of the intensity of the $\dot{P}L_3$ radical (spectrum B) along with some analytical data. There are no correlations of the intensity of the $\dot{P}L_3$ radical with the content of uranium and thorium but an interrelationship is found between the mass loss at 320°C and the content C_{org} and the IR spectral data. Furthermore, as indicated above, the temperatures for the burn-off of the organic matter and for the annihilation of the ESR sites coincide. All these experimental findings suggest that the organophosphorus radicals detected are present in the apatite structure, which permits their displacement in light of the crystal chemical parameters. Unfortunately, the lack of monocrystals in the group of sedimentary apatites prevents definite localization of the radicals in the structure and only hypotheses concerning the site of these radicals may be made. Further studies are required to determine the behavior, interrelationship, and interaction of the organophosphorus radicals, clarify the nature of these radicals, and search for monocrystalline samples such as in the group of sedimentary metamorphic apatites.

The presence of organophosphorus radicals in apatite is a natural occurrence. Apatite participates in biological metabolism and is found in tooth enamel and implanatatory‡ and, thus, lies on the boundary between living and inanimate matter. The formation of inorganic apatite from organic phosphorus has been demonstrated experimentally [20]. The formation of marine phosphorites is related to biogenic activity [21]. The capacity of apatite to interact with organic compounds and adsorb them was noted in 1861 when apatite was used as an adsorbent for the purification of pepsin and later in the chromatographic separation of proteins and nucleic acids. These properties of apatite have specifically led to a broad study of the adsorption of various organic compounds by the mineral component of teeth and bone [22-24], which is important for the prevention of caries and the formation of dental calculus and also for the mechanism of the attachment of organic flotoreagents by apatite in flotation processes [25]. The following properties were found for apatite: 1) a strongly polarized surface, which facilitates active reaction with various reagents (the capacity of apatite to form strong bonds with polar or polarizable molecules has been noted) and 2) the major adsorption sites are the Ca and P positions. The Ca positions bind acid groups, while the P positions bind basic groups.

IR spectroscopy has shown the presence of organic CH_2—COO molecules in "channels" [26] and the adsorption of organic phosphates and polyphosphonates by the apatite surface

†The ENDOR spectra were taken by V. A. Nadolinin at the Institute of Inorganic Chemistry, Siberian Branch, Russian Academy of Sciences on a Varian E109E ESR spectrometer. The ^{31}P MAS-NMR spectra were taken by V. M. Mastikhin at the Institute of Catalysis, Siberian Branch, Russian Academy of Sciences on a Bruker CXP-300 spectrometer.

‡As in Russian original. We assume this to mean implants – Publisher.

has been studied [27, 28]. In our previous work [29], ESR spectroscopy was used to study the organic formyl radical HCO in the structure of synthetic and natural apatite [29], which is characteristic for nonstoichiometric differences with a phosphorus deficiency: Ca/P > 1.67.

The present study indicates that organophosphorus radicals are also present in the structure of natural apatite. Organic matter is a characteristic component of natural phosphorite apatites. The presence of apatite may be due to biological origin or the action of organic solutions on already formed phosphorite under given conditions. Organophosphorus radicals have been detected in apatites of marine and hypergenic origin subjected to the cathagenesis. Such radicals are not found in apatites of young mesozoic and cenozoic phosphorites not subjected to cathagenic transformation. The ESR spectra of organophosphorus radicals disappear upon recrystallization in weathering processes. Thus, radicals are found in marine, cathagenically transformed apatites of the Georgina basin (Table 1, samples 7 and 8) but are lacking in hypergenically recrystallized samples (sample 9).

As noted above, the spectrum of PL_3 rather frequently accompanies the spectrum of the $PO_3^{2-}(Th)_1$ radical, sometimes even in the complete absence of $PO_3^{2-}(U)_1$. The action of organothorium solutions in the genetic history of apatites is possible, resulting in the formation of organophosphorus complexes.

Thus, ESR spectroscopy has been used to detect new radicals with splitting by the ^{31}P nucleus in apatite: phosphinyl, PL_2; phosphoryl, PL_3, and phosphoranyl, PL_4. In contrast to phosphoryl radicals PO_3^{2-} previously described in apatite, organic matter, whose qualitative composition and amount were established by chemical analysis and IR spectroscopy, always accompanies the new radicals in the samples studied. A correlation is observed between the ESR spectral data and the analytical data. These experimental results indicate that the new radicals are organophosphorus complexes with organic molecules having CH bonds in the second coordination sphere. However, the final composition of the radicals has still not been established.

The authors express their deep gratitude to V. M. Mastikhin and V. A. Nadolinin for their interest and assistance in this work.

LITERATURE CITED

1. M. Ya. Shcherbakova, L. G. Gilinskaya, and G. M. Zhidomirov, Molecular Structure and Quantum Chemistry [in Russian], Naukova Dumka, Kiev (1970), pp. 69-75.
2. L. G. Gilinskaya and M. Ya. Shcherbakova, The Physics of Apatite [in Russian], Nauka, Novosibirsk (9175), pp. 7-63.
3. L. G. Gilinskya, Molecular Spectroscopy and X-Ray Diffraction of Minerals [in Russian], Nauka, Novosibirsk (1981), pp. 139-149.
4. L. G. Gilinskaya, The Physical Investigation of Calcium Phosphates [in Russian], Nauka, Novosibirsk (1979), pp. 39-48.
5. L. G. Gilinskaya, Zh. Strukt. Khim., 31, No. 6, 51-58 (1990).
6. V. P. Fadeeva and I. M. Moryakina, Izv. Siber. Otdel. Akad. Nauk SSSR, Ser. Khim., No. 14, issue 6, 113-118 (1981).
7. E. K. Lazarenko, Textbook on Mineralogy [in Russian], Vysshaya Shkola, Moscow (1963).
8. R. A. Young, Trans. N. Y. Acad. Sci., Ser. II, 29, 949-959 (1967).
9. L. G. Gilinskaya, L. M. Krivoputskaya, and L. N. Pospelova, Problems in Theoretical and Genetic Mineralogy [in Russian], Nauka, Novosibirsk (1981), pp. 140-148.
10. D. M. Close, M. Mengeot, and O. R. Gilliam, J. Chem. Phys., 74, No. 10, 5497-5503 (1981).
11. L. G. Gilinskaya and Yu. N. Zanin, Dokl. Akad. Nauk SSSR, 273, No. 6, 1463-1467 (1983).
12. J. H. Levy and W. J. Stuart, Thermochimica Acta, 74, 227-234 (1984).
13. A. I. Danishevskaya, New Methods for the Study of Diffuse Organic Matter [in Russian], Arctic Geology Research Institute, Leningrad (1971), pp. 44-50.
14. R. R. Shagidullin, A. V. Chernova, V. S. Vinogradova,and F. S. Mukhaletov, Atlas of the IR Spectra of Organophosphorus Compounds [in Russian], Nauka, Moscow (1984).
15. C. M. L. Kerr, K. Webster, and F. Williams, J. Phys. Chem., 79, 2650-2662 (1975).
16. A. V. Il'yasov, I. D. Morozova, A. A. Vafina,and M. B. Zuev, ESR Spectra and Stereochemistry of Phosphorus-Containing Free Radicals [in Russian], Nauka, Moscow (1985).

17. D. L. Griscom, E. J. Friebele, K. J. Long, and J. W. Fleming, J. Appl. Phys., 54, No. 7, 3743-3762 (1983).
18. M. A. Veiderma and Kh. N. Veskimyaé, Izv. Akad. Nauk Éstonsk. SSR, Khim., Geol., 20, 57-61 (1971).
19. S. R. Silverman, R. K. Fuyat, and J. D. Weiser, Amer. Miner., 37, Nos. 3/4, 211-222 (1952).
20. J. Lucas and L. Prévót, Comptes Rendus Acad. Sci. (Paris), Ser. II, 292, 1203-1208 (1981).
21. N. V. Shabanina, Litol. Polezn. Iskop., No. 3, 82-88 (1988).
22. R. A. Beele and A. S. Posner, Coll. Intern. C. N. R. S., No. 230, 275-281 (1975).
23. G. Bernardi, Coll. Intern. C. N. R. S., No. 230, 463-465 (1975).
24. H. R. Rawls, T. Bartels, and J. Arends, J. Coll. Interf. Sci., 87, No. 2, 339-345 (1982).
25. R. G. Knubovets and B. M. Maslennikov, Dokl. Akad. Nauk SSSR, 164, No. 2, 387-389 (1965).
26. C. Rey, J. C. Trombe, and G. Montel, Comptes Rendus Acad. Sci. (Paris), 283C, 465-467 (1976).
27. H. R. Rawls and J.Calasso, in: Adsorption on and Surface Chemistry of Hydroxyapatite, Plenum Press, New York (1984), pp. 115-128.
28. D. N. Misra, in: Adsorption on and Surface Chemistry of Hydroxyapatite, Plenum Press, New York (1984), pp. 105-114.
29. L. G. Gilinskaya and M. V. Chaikina, Zh. Strukt. Khim., 20, No. 6, 1120-1122 (1979).
30. B. A. Goodman and J. Raynor, in: Advances in Inorganic Chemistry and Radiochemistry, Vol. 17 (1970), pp. 135-180.